Available online at www.HighTechJournal.org

HighTech and Innovation Journal

ISSN: 2723-9535

Vol. 7, No. 2, June, 2026

Modeling Climate-Driven Attenuation in Next-Generation Wireless Communication Networks

Hasanain A. H. Al-Behadili [1], Nasif Jasim Hadi [2*], Maab Alaa Isamail [1], Shaymaa Abed Hussein [3]

[1] *Department of Electrical Engineering, College of Engineering, University of Misan, Misan, Iraq.*

[2] *Department of Chemical Engineering, College of Engineering, University of Misan, Misan, Iraq.*

[3] *Department of Civil Engineering, College of Engineering, University of Manara, Misan, Iraq.*

Received 12 March 2026; Revised 21 May 2026; Accepted 25 May 2026; Published 01 June 2026

Abstract

Electromagnetic signal propagation is particularly complex in hot regions because it is strongly affected by extreme weather conditions, including temperature, humidity, and dust concentration. This poses a significant challenge for telecommunications operators in network planning and management. The Middle East is an important region for such investigations because of its extreme temperatures, and Iraq provides a representative example. This study aims to evaluate the effects of climatic parameters on signal propagation across different frequency bands, including those used in 4G, 5G, and 6G systems. The analysis employs combined calculations based on signal attenuation and measurements of the most influential weather parameters, particularly temperature, humidity, and dust concentration. This study represents the first multivariable investigation in Iraq covering these three frequency bands while considering the Signal-to-Noise Ratio (SNR), Bit Error Rate (BER), and the feasibility of using Reconfigurable Intelligent Surface (RIS) technology to mitigate climatic effects. The results reveal that temperature has a major effect on path loss, producing attenuation ranging from 0.6 to 2.4 dB/km. The findings also indicate that operation in the sub-terahertz band can be effective over short distances and in indoor environments. During the summer, the SNR may deteriorate significantly, highlighting the need for a climate-aware network management system.

Keywords: Signal to Noise Ratio; Reconfigurable Intelligent Surface; Bit-Error-Rate; mmWave and sub-THz.

1. Introduction

As a result of severe weather conditions, the Middle East faces particular challenges in deploying fifth-generation (5G) and beyond-5G (B5G) communication systems. Iraq experiences frequent dust storms, with particle concentrations exceeding 500 μg/m³ [1], summer temperatures that regularly surpass 50°C, and substantial fluctuations in humidity. Such climatic conditions significantly hinder radio signal propagation, particularly in higher-frequency bands, including millimeter-wave (mmWave) and sub-terahertz (sub-THz) frequencies, which are being investigated for advanced 5G and 6G systems [2]. These harsh conditions affect signal propagation through two primary mechanisms: atmospheric attenuation and thermal stress on devices.

Previous research has examined the effects of climate on signal characteristics. Very-high-frequency bands, such as 5G mmWave, are more sensitive to variations in atmospheric conditions than lower sub-6 GHz bands. Studies have

* Corresponding author: nsf_jsm@uomisan.edu.iq

https://doi.org/10.28991/HIJ-2026-07-02-09

reported that higher-frequency signals experience substantial path loss due to humidity and atmospheric temperature, factors that must be considered when deploying networks in arid regions [3]. It has also been shown that elevated temperature and humidity levels can reduce the Signal-to-Noise Ratio (SNR) from 35 dB to 18 dB, thereby significantly increasing the Bit Error Rate (BER) [4]. In addition to effects on the propagation medium, Iraq's physical communication infrastructure faces significant thermal challenges. Thermal expansion can alter the refractive index and radius of curvature of glass fibers in the fiber-optic backhaul networks supporting mobile towers, thereby causing signal dispersion [5].

In Middle Eastern regions, devices such as solar-powered stations and wireless nodes experience a 0.3%–0.5% reduction in power-conversion efficiency for every degree Celsius increase in temperature above 25°C, which threatens the reliability of off-grid communication systems. Other studies focusing on the reliability of wireless links in arid environments have similarly demonstrated the adverse effects of extreme heat on wireless nodes [6, 7].

Amajama et al. [8] have further examined the effect of atmospheric temperature on signal power, reporting an inverse relationship between temperature and mobile signal strength. Similarly, Boano et al. [9] suggested that fluctuations in temperature can affect the reliability of wireless communications. Luomala & Hakala [10] also demonstrated, using a global reference, that temperature is the dominant environmental factor influencing wireless sensor networks in outdoor environments.

Global efforts have sought to present studies that clarify the effects of climate change on communication infrastructure and signal propagation, including the 2022 and 2024 updates of the Intergovernmental Panel on Climate Change (IPCC) and the work of the ITU-T Focus Group [11]. The International Telecommunication Union has established global standards for incorporating climate-resilient designs into smart-city infrastructure in order to prevent signal degradation caused by heat. Although current standards are based primarily on observations from temperate regions, the International Telecommunication Union has recognized the need for region-specific propagation models. The absence of such models can lead to overdesigned systems, inaccurate link-budget calculations, or unplanned service interruptions during extreme weather events.

Several studies have been conducted across Iraqi governorates, including those reported in [12–14], presenting various types of measurements and results. Conventional propagation models generally assume normal atmospheric conditions and therefore neglect temperature-dependent atmospheric refraction, humidity-induced absorption, dust-particle scattering and attenuation, and the combined nonlinear effects of climatic factors. Furthermore, the potential of Reconfigurable Intelligent Surfaces (RIS) as a compensatory mechanism in harsh desert environments remains uncertain.

Recent studies have shown that environmental and climatic conditions, including extreme temperature, humidity, rainfall, and dust storms, have particularly important effects on emerging 5G and beyond systems operating at high frequencies [15, 16]. Existing literature has mainly emphasized individual atmospheric factors, such as rainfall attenuation, dust-induced path loss, and humidity effects on mmWave propagation, with limited attention given to integrated climate-aware modeling in arid Middle Eastern environments. Moreover, although many studies have examined weather-related attenuation in specific regions, most models were developed under temperate or generalized urban conditions and do not fully capture the extreme thermal conditions experienced in Iraq and neighboring Gulf countries, where summer temperatures regularly exceed 50°C [17, 18].

This reveals a critical research gap concerning the combined effects of high temperature and atmospheric variability on mobile communication performance in Middle Eastern climates. To address this gap, the present study proposes an integrated climate-sensitive propagation framework that relates temperature increases and atmospheric attenuation to key communication performance indicators, including path loss and Signal-to-Noise Ratio (SNR). Unlike previous studies, the proposed methodology specifically focuses on high-temperature Middle Eastern environments and climate-resilient communication infrastructure. This paper extends the projects presented in [19–21] and makes the following contributions:

- ***Climate-Sensitive Diffusion Model:*** A physics-based model that includes temperature, humidity, and dust attenuation factors calibrated to Iraqi desert conditions in multiple frequency bands.
- ***Multi-Band Analysis:*** A comparative assessment to quantify the increased vulnerability at higher frequencies in the 6 GHz (3.5 GHz), millimeter wave (28 GHz), and terahertz (140 GHz) sub bands.
- ***RIS Compensation Analysis:*** Quantification of RIS gain, gain for restoration of NLOS mmWave links under extreme weather conditions, showing 48 dB gain and 162% coverage extension.
- ***BER Performance:*** End-to-end BER analysis of QPSK and 16-QAM modulations during climate-induced degradation, imposing practical limits on range.
- ***Sub-THz Extension:*** Assessing the feasibility of the 140 GHz band and demonstrating that NLOS is not practical in desert conditions.

- ***Comprehensive Validation:*** Statistical validation using realistic synthetic and noise-distorted data sets, with ablation studies that confirm the contribution of each component.
- ***Complexity Analysis:*** Blogging analysis shows the complexity of real-time deployment.

2. System and Propagation Model

The model combines the fundamental theory of electromagnetic propagation with environmental parameters to predict the performance of sub-6 GHz, millimeter-wave (mmWave), and sub-terahertz (sub-THz) communication links. The proposed approach incorporates free-space path loss calculations, line-of-sight (LOS) and non-line-of-sight (NLOS) propagation effects, climate-induced attenuation due to temperature, humidity, and dust, Signal-to-Noise Ratio (SNR) analysis, Bit Error Rate (BER) estimation, and Reconfigurable Intelligent Surface (RIS) enhancement. Figure 1 presents a flowchart illustrating the complete computational workflow.

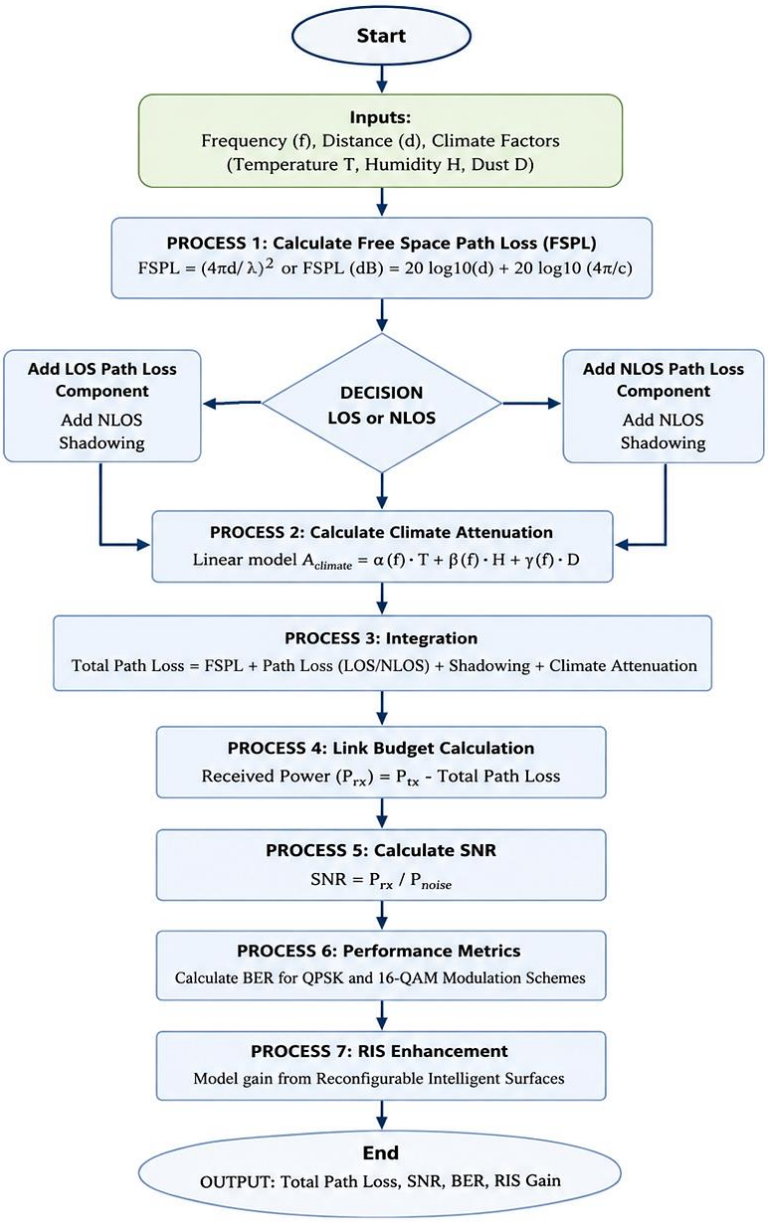

Figure 1. System flow chart

The system flowchart begins with the system parameters, including frequency, distance, transmit power, and antenna gains, together with environmental conditions such as temperature, humidity, and dust concentration. These inputs are processed through successive propagation and system models to generate performance metrics, including total path loss, received SNR, and BER.

The baseline free-space path loss (FSPL) is derived from the Friis transmission equation:

$$P_r = P_t G_t G_r \left(\frac{\lambda}{4\pi d}\right)^2 \quad (1)$$

Real-world propagation environments exhibit significant differences between line-of-sight (LOS) and non-line-of-sight (NLOS) conditions. 3GPP-inspired models have been adopted:

LOS Path Loss:

$$PL_{LOS}(d) = FSPL(d,f) + \eta_{LOS} \quad (2)$$

NLOS Path Loss:

$$PL_{NLOS}(d) = FSPL(d,f) + 20\log_{10}(d) + \eta_{NLOS} \quad (3)$$

Then**,** the climate-dependent attenuation is modeled as a linear combination of environmental factors:

$$L_{climate} = \alpha_T T + \alpha_H H + \alpha_D D \quad (4)$$

where, T is temperature in °C, H is relative humidity in % and Dis dust concentration in μg/m³. The coefficients α_T, α_H, and α_D They are frequency-dependent and calibrated based on atmospheric physics and empirical measurements in desert environments (see Table 1).

Table 1. Calibrated coefficients for Iraqi desert conditions

Frequency Band	Temp Coeff (αT)	Humidity Coeff (αH)	Dust Coeff (αD)
3.5 GHz (sub-6 GHz)	0.02 dB/°C	0.01 dB/%	0.002 dB per μg/m³
28 GHz (mmWave)	0.05 dB/°C	0.03 dB/%	0.01 dB per μg/m³
140 GHz (sub-THz)	0.08 dB/°C	0.05 dB/%	0.02 dB per μg/m³

The recording above shows that at 28 GHz, a dust storm with a concentration of 500 μg/m³ results in 5 dB additional attenuation, whereas at 140 GHz, the same dust contributes 10 dB.

2.1. Complete Path Loss Model

The total path loss combining all effects is:

$$PL_{total}(d,f,T,H,D,LOS) = FSPL(d,f) + \Delta_{NLOS}(d,LOS) + L_{climate}(T,H,D) + \eta \quad (5)$$

where, $\Delta_{NLOS}(d,LOS) = 0$ if LOS $20\log_{10}$(d) if NLOS cases, Δ represents residual shadowing effects not captured by climate terms.

2.2. Link Budget and SNR

The received power is given by:

$$P_r = P_t + G_t + G_r - PL_{total} \quad (6)$$

where, P_t is transmitted power (30 dBm typical for base stations for macro cells); G_t, G_r are antenna gains (15 dB each, typical for directional antennas).

The noise power is:

$$N = -174 + 10\log_{10}(B) + NF \quad (7)$$

where, B is bandwidth (20 MHz for sub-6 GHz, 100 MHz for mmWave and sub-THz), NF is noise figure (7 dB typical for receiver front-end).

The signal-to-noise ratio is:

$$SNR = P_r - N \quad (8)$$

This SNR determines the achievable data rate and modulation scheme.

2.3. Bit Error Rate Models

For QPSK modulation, the bit error probability in AWGN is:

$$BER_{QPSK} = Q\left(\sqrt{2\gamma}\right) \tag{9}$$

where, γ = 10^SNR/10 is the linear SNR and Q(x) is the Gaussian Q-function:

$$Q(x) = \frac{1}{\sqrt{2\pi}}\int_x^{\infty} e^{-t^2/2}\,dt = \frac{1}{2}\text{erfc}\left(\frac{x}{\sqrt{2}}\right) \tag{10}$$

For 16-QAM modulation, the exact BER expression is:

$$BER_{16QAM} = \frac{3}{8}Q\left(\sqrt{\frac{4\gamma}{5}}\right) + \frac{2}{8}Q\left(3\sqrt{\frac{4\gamma}{5}}\right) + \frac{1}{8}Q\left(5\sqrt{\frac{4\gamma}{5}}\right) \tag{11}$$

For practical purposes, the dominant first term provides a good approximation:

$$BER_{16QAM} \approx \frac{3}{8}Q\left(\sqrt{\frac{4\gamma}{5}}\right) \tag{12}$$

2.4. RIS-Assisted Link

A Reconfigurable Intelligent Surface (RIS) comprises M passive reflecting elements that can introduce phase shifts to combine signals coherently at the receiver. For an ideal RIS with optimal phase configuration, the effective power gain is:

$$G_{RIS} = 20\log_{10}(M) \tag{13}$$

This gain arises from the coherent combining of signals from all M paths. In practice, losses due to element efficiency, phase quantization, and mutual coupling reduce this gain by 1-3 dB.

The RIS-compensated path loss becomes:

$$PL_{RIS} = PL_{total} - G_{RIS} \tag{14}$$

For M = 256 elements, the theoretical gain is:

$$G_{RIS} = 20\log_{10}(256) = 20 \times 2.408 = 48.16 \text{ dB} \tag{15}$$

This substantial gain can potentially restore severely attenuated NLOS links to usable levels.

3. Results and Discussion

Climate data were extracted from NASA POWER and NOAA Climate Data Online databases. Various parameters were taken to show their effects on signal propagation, mainly temperature, humidity, and dust.

Figure 2 shows the path loss for three different frequencies, e.g., 3.5 GHz (panel a), 28 GHz (panel b), and c for 140 GHz. The colored scattered records are using LOS (bold) and NLOS (light). These come with two curves using the free space model with the model in Equation 5 (continuous line), and the dotted lines are for FSPL and NLOS, in addition to the climate model using median records.

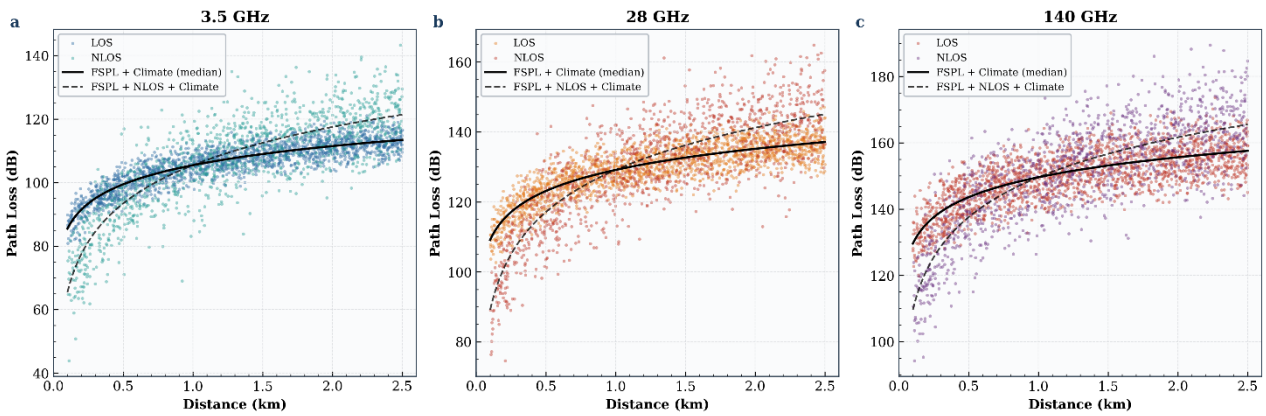

Figure 2. Path loss vs. distance for three frequencies: 3.5 GHz, 28 GHz, 140 GHz (T= 42° C, H =25 %, D= 250 µg/m^3)

Figure 3 explains the effect of the average temperature of Iraq (according to officials) on path loss using different frequencies. These were examined for 1 km, 35% humidity, in addition to 60% LOS, 40% NLOS, and a dust/particulate of 250 µg/m³. Additionally, a linear least-squares fit (1st-degree polynomial) was performed on the temperature and path losses that were provided.

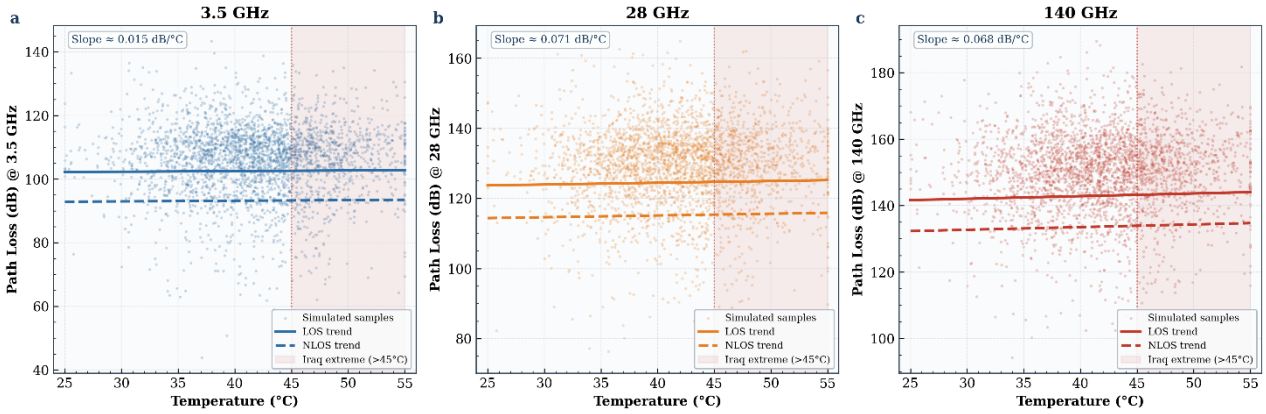

Figure 3. Temperature effect on path loss at 3.5 GHz, 28 GHz and 140 GHz. (d= 1km, H = 25%, D= 250 µg/m^3, 60% LOS, 40% NLOS)

Contour heatmaps for climate attenuation filled with data on temperature vs. humidity (panels a, b, c) and temperature with dust concentration (panels d, e, f) are shown in Figure 4. The signal-to-noise ratio is one of the most important parameters in the assessment of communication systems. It is mostly affected by path loss. Furthermore, Reconfigurable Intelligent Surfaces (RIS) technology is used to adapt radio surfaces to the propagation environment and to enhance the performance of 5G/6G signal propagation, in particular.

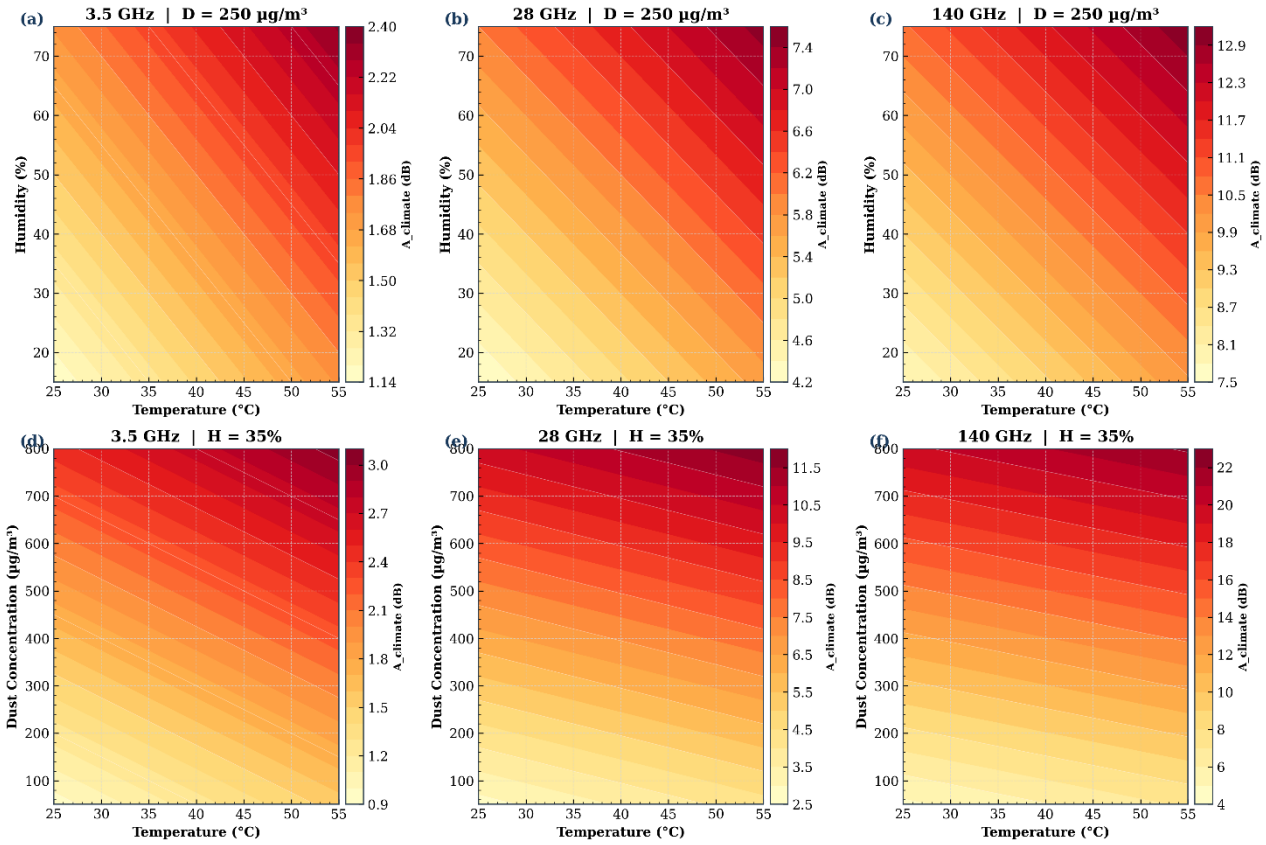

Figure 4. Climate attenuation (dB) heatmaps; (temperature X Humidity (top), temperature X dust (bottom))

Figure 5(a) presents the resulting SNR, including climate-related path-loss effects under line-of-sight (LOS) and non-line-of-sight (NLOS) conditions, over distances of up to 2.5 km. Several scenarios are considered, including LOS

and NLOS conditions with and without RIS. The cases with RIS are shown in green, while those without RIS are represented by red scattered points. The SNR thresholds for QPSK and QAM were set at 5 dB and 15 dB, respectively. Figure 5(b) presents the cumulative distribution of the SNR values used in the analysis.

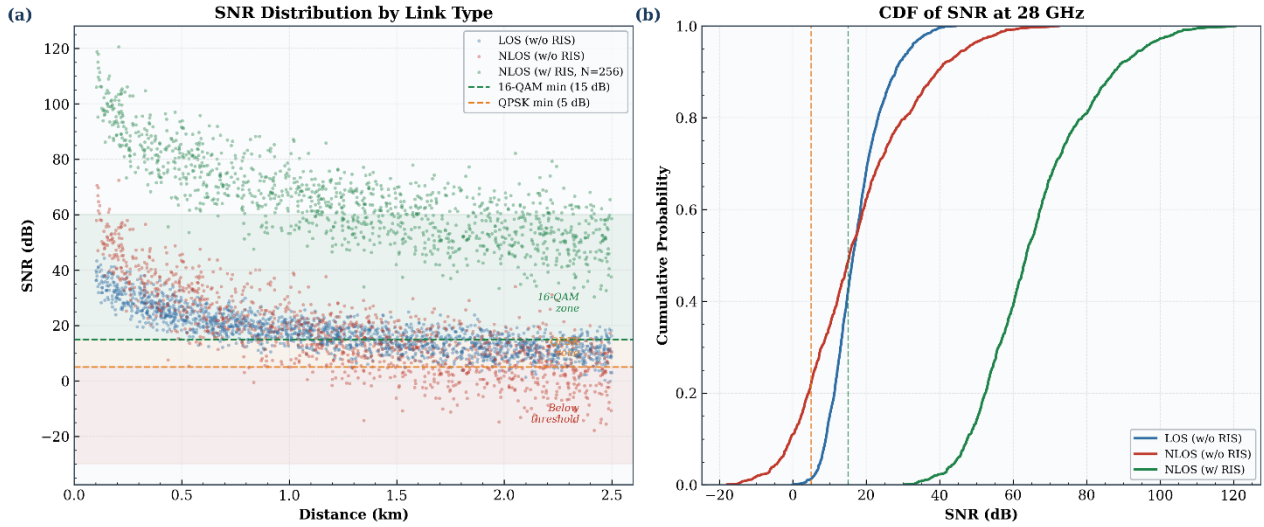

Figure 5. SNR vs. distance at 28 GHz: LOS, NLOS, and RIS- enhanced links

Figure 6 presents the Bit Error Rate (BER) analysis for QPSK and 16-QAM at 28 GHz under Iraq's climatic conditions. In Figure 6(a), the theoretical results indicate that 16-QAM requires a higher SNR. Figure 6(b) illustrates the variation in BER with distance for both modulation schemes, with and without RIS. A BER value of 10^{-3} was used as the reference threshold for evaluating the results. QPSK exhibits higher BER values than 16-QAM.

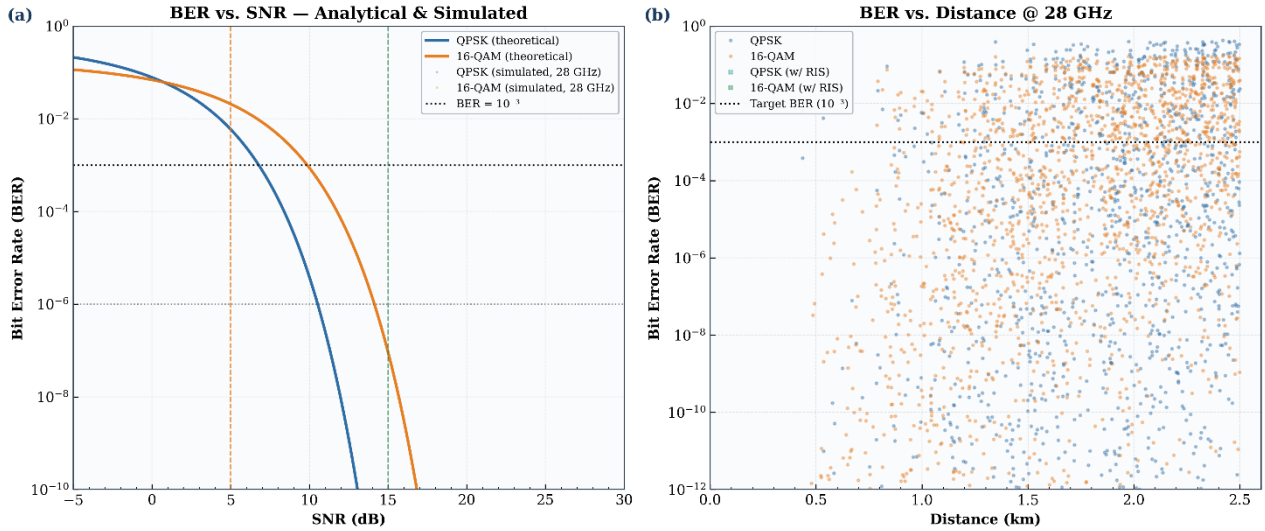

Figure 6. Bit error rate analysis: QPSK AND 16-QAM at 28 GHZ in Iraq

To examine the impact of RIS at millimeter-wave frequencies, particularly 28 GHz, Figure 7(a) presents the variation in SNR with distance. The results show a clear improvement in SNR when RIS is employed. Further evidence is provided in Figure 7(b), where RIS produces a noticeable reduction in outage probability with increasing distance compared with propagation without RIS. The tested RIS configuration consists of 256 reflecting elements. However, Figure 7(c) shows that increasing the number of reflecting elements increases the RIS gain and consequently reduces path loss.

Figure 8 presents a statistical comparison of the three frequency bands. Box plots were used to visualize the distributions of Signal-to-Noise Ratio (SNR) and path loss. The blue lines represent the median values in each box, while the white diamonds indicate the mean values of the distributions. In addition, circular markers represent the extreme values. As shown in Figure 8(a), the frequency dependence of path loss, combined with Iraq's climatic conditions, makes operation at sub-terahertz frequencies particularly sensitive. Figure 8(b) also shows that SNR decreases as frequency increases. This effect is more pronounced at 140 GHz, where the SNR values fall below 5 dB, which is the adopted threshold for QPSK.

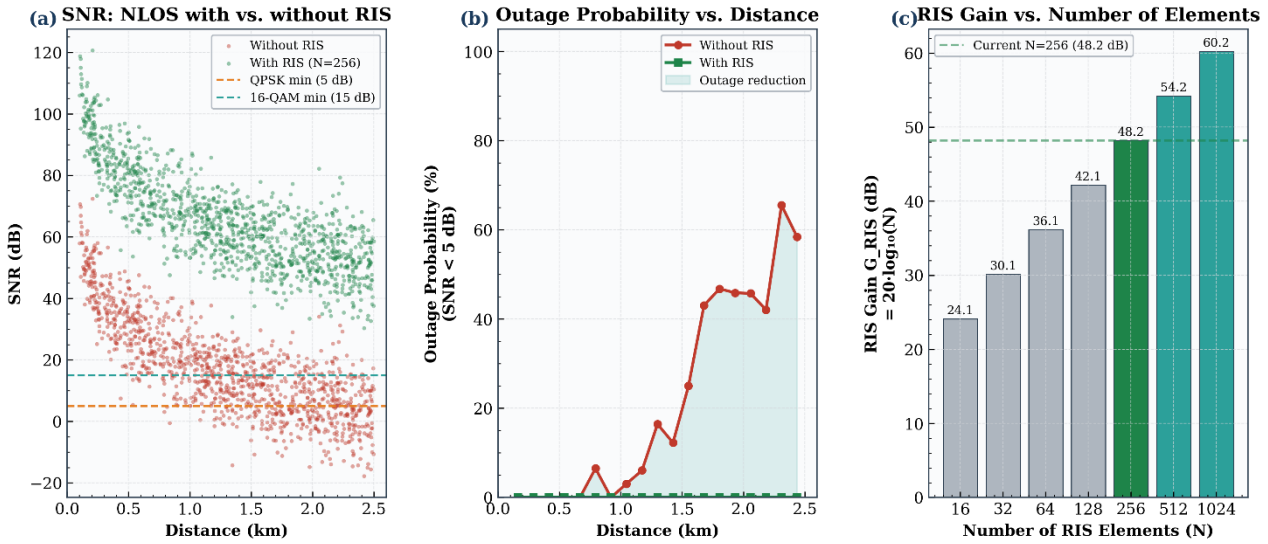

Figure 7. RIS impact on 28 GHz NLOS links (N= 256 elements, G_RIS=48.2 dB)

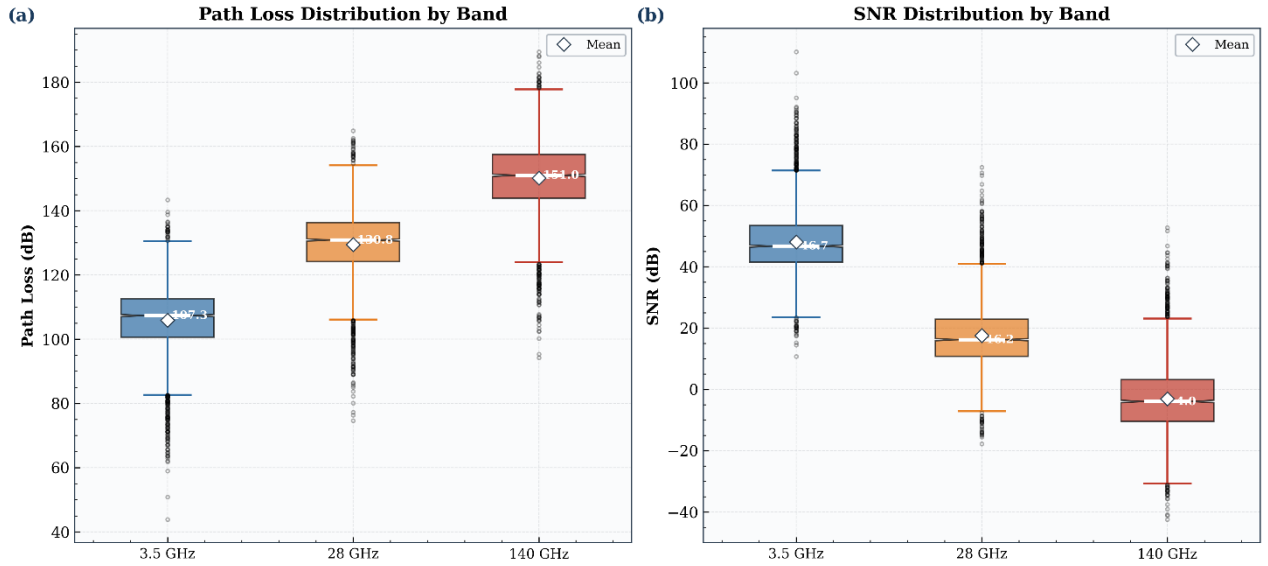

Figure 8. path loss and SNR distribution across frequency bands (3.5 GHz, 28 GHz, 140 GHz, Iraq climate dataset, n=3000)

Iraq experiences frequent dust storms; therefore, it is important to examine the effects of dust on signal parameters. The dust coefficient values are presented in Table 1. As shown in Figure 9(a), there is a linear relationship between path loss and dust concentration. Five different categories of dust concentration are presented in two columns corresponding to line-of-sight (LOS) and non-line-of-sight (NLOS) propagation at 28 GHz. In Figure 9(b), the SNR thresholds for QPSK and QAM are indicated by green and red dotted lines, respectively. An inverse relationship is observed between the dust concentration categories and the SNR values.

The feasibility of using sub-terahertz frequencies across Iraqi territories was also evaluated, as shown in Figure 10. Although this frequency band is sensitive to molecular absorption, it is highly important because of its potential application in 6G mobile communications. A dataset containing 3,000 samples was used to generate the scatter plots in Figure 10(a), where LOS propagation is shown in blue and NLOS propagation in red to illustrate SNR variability with distance. LOS propagation produces positive SNR values, but only over shorter distances. In contrast, the SNR values under NLOS conditions fall below the adopted threshold.

Figure 10(b) illustrates how increasing dust concentration affects SNR values above the threshold, i.e., SNR ≥ 5 dB. Two columns are used to represent LOS and NLOS conditions, both of which are adversely affected by increasing dust concentration. Figure 10(c) provides a practical representation of the effect of temperature on the maximum coverage distance. The results clearly show that, during summer, the maximum coverage may decrease to less than 650 m. This result was obtained for a dust concentration of 250 μg/m³ and a humidity level of 35%, considering only SNR values above the threshold.

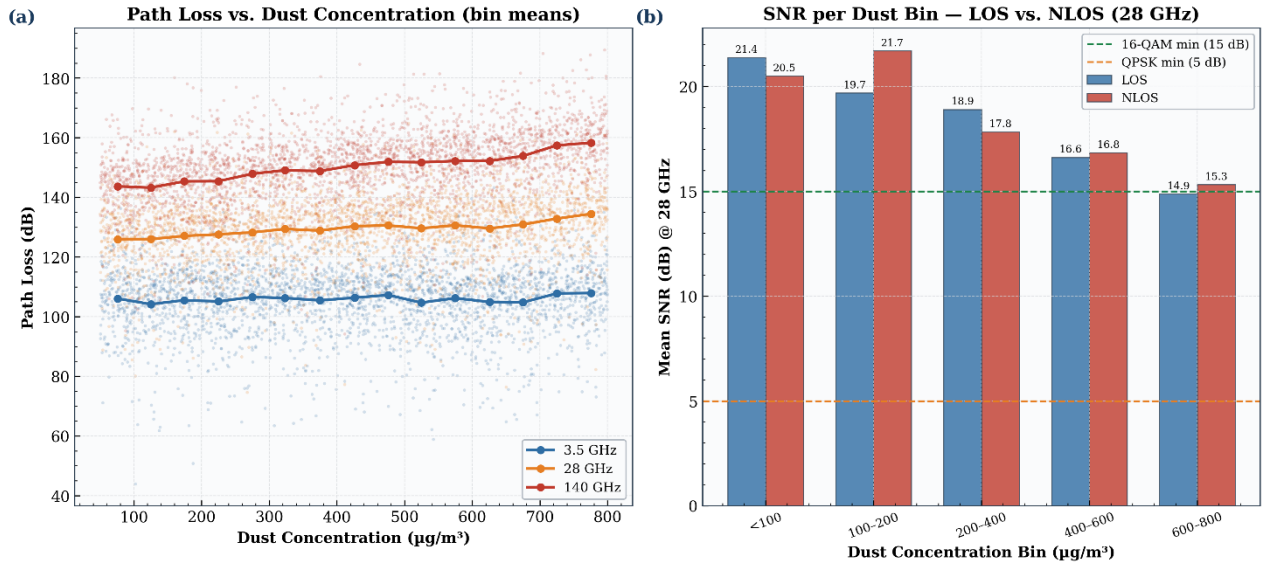

Figure 9. Dust concentration effect on path loss and SNR (Iraq sandstorm conditions: 50- 800 µg/m^3)

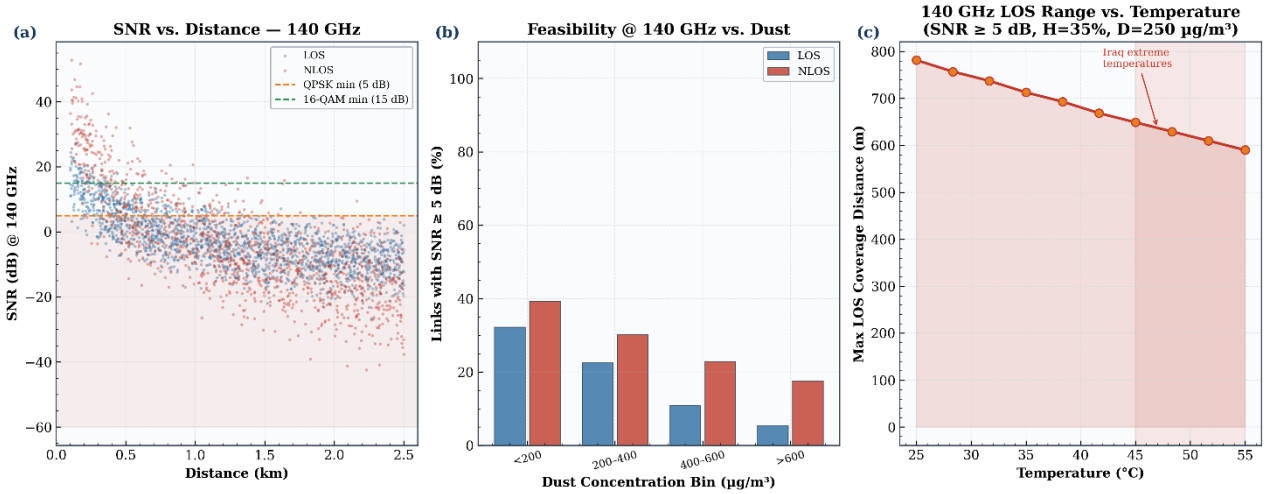

Figure 10. Sub-THz (140 GHz) feasibility in Iraqi desert environment dust, temperature and distance impact

To get knowledge about the effect of each issue on the signal propagation, an ablation study is used as explained in Figure 11. RMSE is employed to show the gap between the predictions of the proposed model and simulated noisy measurements. An additive process in which parts are added one at a time according to their physical intricacy:

(1) FSPL

(2) Shadowing related to LOS/NLOS.

(3) The climate attention method.

(4) RIS gain.

Noise measurement using the following mathematical expression

$$\text{Measured\_Path loss} = \text{Path loss at 28GHz} + U \quad (16)$$

where, $U \sim N(0, 1.5^2)$ dB, constituting a realistic uncertainty field measurement.

Panel (a) presents the four evaluated categories, with the RMSE value displayed above each corresponding bar in decibels. The FSPL model produces the highest RMSE. The physical relationship between the climatic parameters, including temperature, humidity, and dust concentration, and signal propagation in the Iraqi environment is confirmed by incorporating the attenuation caused by these factors, which results in a noticeable reduction in RMSE. The green bar represents RIS compensation and shows the greatest improvement. Panel (b) reorganizes the same four RMSE values to clearly identify each value and emphasize the progressive enhancement achieved at successive stages of the model. Overall, Figure 11 is important for establishing the relative contributions of propagation geometry, climate-induced attenuation, and RIS compensation, particularly in regions exposed to extreme temperatures. The ablation analysis also supports the proposed model architecture.

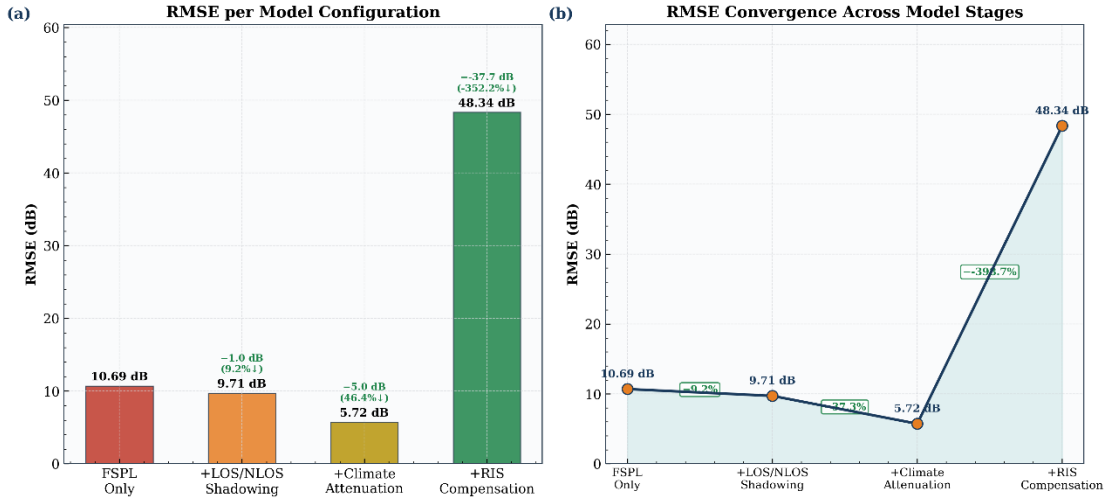

Figure 11. Ablation study: RMSE contribution of each model component (28 GHz, Iraq climate dataset)

The overall effects of Iraq's environmental parameters, including temperature, dust concentration, and humidity, on signal propagation across three frequency bands are ultimately presented in a six-panel figure. Figure 12(a) illustrates the variation in SNR with temperature, with the Iraqi temperature range highlighted in light orange. The SNR decreases across all three frequencies within this range, while dust concentration and humidity are maintained at specified values. Figure 12(b) shows the effect of humidity at 42°C and reveals similar trends. However, a clear difference is observed when dust concentration is treated as the variable at 42°C and 35% humidity, as the SNR becomes weaker at the lower frequency values. All results correspond to a transmission distance of 1 km.

To examine temperature-stratified excess loss and the relationships among variables, Figure 12(d) presents a correlation matrix for the six key variables investigated. Figure 12(e) shows the average excess path loss above FSPL, in decibels, for five selected temperature clusters centered at 28.5, 35.0, 40.5, 45.5, and 51.5°C. The shaded area in Figure 12(e) provides an integrated visual representation of the cumulative additional attenuation across the temperature range. Finally, Figure 12(f) presents a two-dimensional heatmap of the 28 GHz LOS SNR as a joint function of environmental temperature and dust concentration, with humidity fixed at H = 35% and distance fixed at d = 1 km. The diagonal orientation of the constant-SNR contours across the temperature–dust plane illustrates the cumulative nature of the climatic attenuation model. This confirms that dust concentration and temperature can impose additive and approximately linear penalties on 28 GHz link quality under Iraqi environmental conditions.

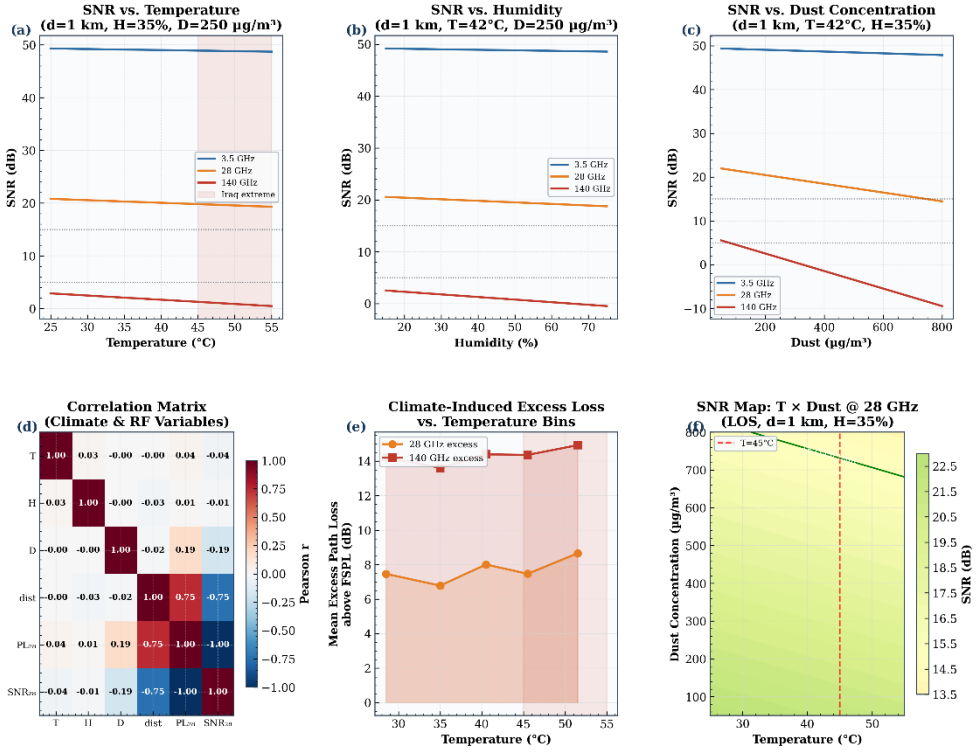

Figure 12. Climate sensitivity dashboard, Iraq desert mobile communications temperature, humidity, dust impact on multi-band signal performance

Figure 13 provides the concluding quantitative summary of the propagation analysis by translating the physics-based climate attenuation model into engineering parameters directly relevant to link-budget design. This is achieved by decomposing the total path loss into free-space path loss, climate-induced attenuation, and fading components, and then tracing the power flow to estimate the overall link budget.

Each of the three side-by-side stacked bar charts in Figure 13(a), representing one frequency band, divides the total path loss into three vertically stacked components: climate attenuation (orange), free-space path loss (blue), and a representative one-standard-deviation LOS shadowing contribution of 3 dB (red). The total path loss is indicated above each bar, while the value of each component is displayed in white within its corresponding segment.

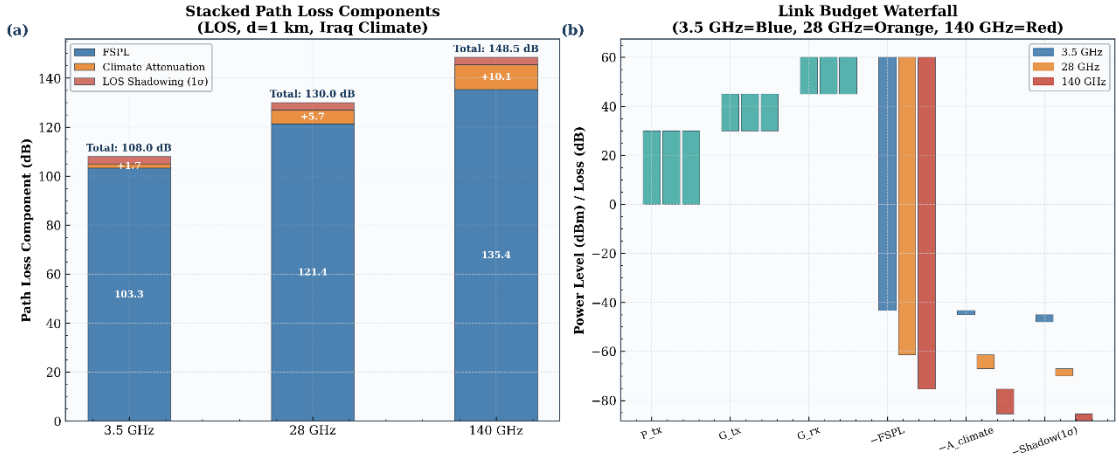

Figure 13. Path loss component breakdown and link budget summary (d= 1km, T= 42 °C, D= 250 µg/m^3)

Of particular interest is the increase in the proportion of climate-induced attenuation relative to FSPL as frequency rises. At 3.5 GHz, climate attenuation represents only a small fraction of the total loss, whereas at 140 GHz, it accounts for a substantially larger proportion. This finding emphasizes that climate-related corrections become increasingly important at higher frequencies.

Figure 13(b) presents a waterfall chart illustrating the cumulative power gains and losses along the communication link for the three frequencies, each represented by a distinct color. The chart includes transmitted power and antenna gains as upward bars, and free-space path loss, climate attenuation, and fading as downward bars. FSPL is the dominant loss component at all frequencies, followed by climate-induced attenuation and shadowing, providing useful information for radio-frequency planning. The results presented in this figure provide telecommunications engineers and infrastructure planners with the information required to evaluate link margins, select suitable frequency bands, and determine appropriate fade margins for mobile communication systems operating under Iraq's extreme temperature conditions.

4. Conclusion

This study analyzed the effects of Iraq's extreme-temperature desert climate on wireless signal propagation across sub-6 GHz, millimeter-wave (mmWave), and sub-terahertz frequency bands associated with current 5G and future 6G systems. Using climate-aware propagation modeling together with environmental data representative of Iraqi conditions, the results show that extreme atmospheric conditions substantially degrade communication performance through three primary mechanisms: temperature-dependent atmospheric absorption, humidity-induced molecular attenuation, and dust-particle scattering. The analysis further demonstrated that these environmental effects become progressively more severe as the operating frequency increases, with mmWave and sub-THz bands exhibiting significantly greater sensitivity than conventional cellular frequencies. Specifically, frequencies below 6 GHz maintain relatively stable propagation performance under harsh climatic conditions, whereas frequencies above 28 GHz experience substantial increases in attenuation, reduced received signal strength, and lower Signal-to-Noise Ratio (SNR), particularly during periods of elevated humidity and dust concentration.

The findings further indicate that mmWave bands can still support practical urban 5G deployment in Iraq if adaptive mitigation techniques, including optimized link budgeting, non-line-of-sight (NLOS) management, beamforming, and Reconfigurable Intelligent Surface (RIS) compensation, are employed. RIS-assisted propagation enhancement demonstrated considerable potential for mitigating climate-related degradation by improving received power and extending coverage under challenging environmental conditions. However, several practical deployment challenges must be considered, particularly in harsh desert environments such as Iraq. These include cost, alignment, beam-steering accuracy, maintenance requirements, and environmental durability.

Overall, the proposed climate-dependent propagation framework provides a practical basis for designing climate-resilient wireless networks in Iraq and may also be applicable to similar regions across the Middle East. Future research will focus on developing nonlinear atmospheric models and real-time, environment-adaptive propagation prediction techniques to further improve communication reliability under extreme climatic conditions.

5. Declarations

5.1. Author Contributions

Conceptualization, H.A.H.A.-B. and N.J.H.; methodology, H.A.H.A.-B. and N.J.H.; software, N.J.H.; validation, H.A.H.A.-B., M.A.I., and S.A.H.; formal analysis, N.J.H. and H.A.H.A.-B.; investigation, H.A.H.A.-B., N.J.H., and M.A.I.; resources, M.A.I. and S.A.H.; data curation, N.J.H. and M.A.I.; writing—original draft preparation, H.A.H.A.-B. and N.J.H.; writing—review and editing, H.A.H.A.-B., N.J.H., M.A.I., and S.A.H.; visualization, N.J.H.; supervision, H.A.H.A.-B.; project administration, H.A.H.A.-B. All authors have read and agreed to the published version of the manuscript.

5.2. Data Availability Statement

The data presented in this study are available on request from the corresponding author.

5.3. Funding

The authors received no financial support for the research, authorship, and/or publication of this article.

5.4. Acknowledgments

The authors are very grateful for the valuable help from the Iraqi Meteorological Organisation and Seismology, the Iraqi Ministry of Science and Technology, the National Aeronautics and Space Administration (NASA), and the European Organisation for the Exploitation of Meteorological Satellites (EUMETSAT) for offering mapping and data on meteorological parameters.

5.5. Institutional Review Board Statement

Not applicable.

5.6. Informed Consent Statement

Not applicable.

5.7. Declaration of Competing Interest

The authors declare that they have no known competing financial interests or personal relationships that could have appeared to influence the work reported in this paper.

6. References

[1] Ismail, R. R., Halos, S. H., & Al-Abudi, B. Q. (2025). Detection of the most frequent sources of dust storms in Iraq during 2020–2023 using space tools. Kuwait Journal of Science, 52(1), 100328. doi:10.1016/j.kjs.2024.100328.

[2] Ahmed, A. M., Majeed, S. A., & Dawood, Y. S. (2022). 6G THz-band facing propagation and atmospheric absorption losses. 4th International Conference on Communication Engineering and Computer Science (CIC-COCOS'22), 162–168.

[3] Ratul, R. H., Mehedi Zaman, S. M., Chowdhury, H. A., Hassan Sagor, M. Z., Kawser, M. T., & Muntasir Nishat, M. (2023). Atmospheric Influence on the Path Loss at High Frequencies for Deployment of 5G Cellular Communication Networks. 2023 14th International Conference on Computing Communication and Networking Technologies, ICCCNT 2023, 16(4), 12–25. doi:10.1109/ICCCNT56998.2023.10307972.

[4] Sabah, S., Hussain, R. T., Duishobekovich, M. U., Jawad, H. M., & Abbas, I. (2025). A Pathway to Ultra-Fast Data Transmission for Next-Generation Networks through Terahertz Communication in 6G. Iranian Journal of Information Processing and Management, 40(1), 1179–1212. doi:10.22034/jipm.2025.728403.

[5] Mohammed, A. A., & Qasmarrogy, G. A. (2022). Thermal effect on the optical signal of fiber optics networks. International Review of Applied Sciences and Engineering, 13(2), 164–173. doi:10.1556/1848.2021.00328.

[6] Dehwah, A. H., Mousa, M., & Claudel, C. G. (2015). Lessons learned on solar powered wireless sensor network deployments in urban, desert environments. Ad Hoc Networks, 28, 52-67. doi:10.1016/j.adhoc.2015.01.013.

[7] Vighio, A. A., Zakaria, R., Ahmad, F., & Aminuddin, E. (2025). Real-Time Monitoring and Development of a Localized OTTV Equation for Building Energy Performance. Civil Engineering Journal, 11(2), 544–564. doi:10.28991/CEJ-2025-011-02-09.

[8] Amajama, J., Ibrahim, A. T., & Akwagiobe, J. U. (2023). Influence of atmospheric temperature on the signal strength of mobile phone communication. Communication in Physical Sciences, 9(4), 717-737.

[9] Boano, C. A., Cattani, M., & Römer, K. (2018). Impact of temperature variations on the reliability of LoRa—An experimental evaluation. In Proceedings of the 7th International Conference on Sensor Networks (SENSORNETS 2018), 39–50.doi:10.5220/0006605600390050.

[10] Luomala, J., & Hakala, I. (2015). Effects of temperature and humidity on radio signal strength in outdoor wireless sensor networks. Proceedings of the 2015 Federated Conference on Computer Science and Information Systems, FedCSIS 2015, 5, 1247–1255. doi:10.15439/2015F241.

[11] ITU. (2015). Information and communication technologies for climate change adaptation in cities. International Telecommunication Union, ITU-T Technical Report. Available online: https://www.itu.int/en/ITU-T/focusgroups/ssc/Pages/default.aspx (accessed on May 2026).

[12] Al-Kadhimi, A. M. (2024). Investigating 5G Wireless Networks Deployment with Diverse Frequency Bands for Basra City. Diyala Journal of Engineering Sciences, 17(4), 56–74. doi:10.24237/djes.2024.17404.

[13] Khazaal, H. F., Saadoon, H., & Jamel, T. (2022). 5G with millimeter waves The Effects Of Different Weather Conditions On 5G Millimeter Waves Propagations at 38 GHz and 73 GHz For Kut-City in Iraq: 5G millimeter waves. Wasit Journal of Engineering Sciences, 10(2), 20-33. doi:10.31185/ejuow.Vol10.Iss2.274.

[14] Sideeq, Z. A. (2019). An investigation of 5G propagation models/weather effects. Master's thesis, College of Electronics Engineering, University of Mosul, Mosul, Iraq.

[15] Hemadeh, I. A., Satyanarayana, K., El-Hajjar, M., & Hanzo, L. (2017). Millimeter-wave communications: Physical channel models, design considerations, antenna constructions, and link-budget. IEEE Communications Surveys & Tutorials, 20(2), 870-913. doi:10.1109/COMST.2017.2783541.

[16] Rappaport, T. S., Xing, Y., MacCartney, G. R., Molisch, A. F., Mellios, E., & Zhang, J. (2017). Overview of Millimeter Wave Communications for Fifth-Generation (5G) Wireless Networks-With a Focus on Propagation Models. IEEE Transactions on Antennas and Propagation, 65(12), 6213–6230. doi:10.1109/TAP.2017.2734243.

[17] Al-Hourani, A., & Gomez, K. (2018). Modeling Cellular-to-UAV Path-Loss for Suburban Environments. IEEE Wireless Communications Letters, 7(1), 82–85. doi:10.1109/LWC.2017.2755643.

[18] Dastkhosh, A. R., Mehbodniya, A., Webber, J., Naseh, M., Dadras Jedi, M., & Lin, F. (2025). Small Dual Polarized UWB Antenna and Its Array Analysis for 5G/6G Applications. Emerging Science Journal, 9(6), 2929–2945. doi:10.28991/ESJ-2025-09-06-04,.

[19] Hazim, H. T., Al-Behadili, H. A. H., Kareem, T. A., & Jabbar, M. K. (2020). Design of mobile communication system for emergency services. International Journal of Interactive Mobile Technologies, 14(13), 238–247. doi:10.3991/ijim.v14i13.14623.

[20] Pham, T. T. H., Nguyen, T. T. T., Trinh, T. T., Pham, M. H., & Ngoc, T. T. B. (2025). Novel Management Model for Leveraging Leadership for Successful Digital Transformation in Telecommunications Enterprises. HighTech and Innovation Journal, 6(2), 363–383. doi:10.28991/HIJ-2025-06-02-01.

[21] Abdullrazaq, N. A., & Hasan, H. A. (2024). Predicting The Path Loss at the Receiver for 4G Communications 2600MHz Using Mathematical Model in Amara City. 2024 International Symposium of Systems, Advanced Technologies and Knowledge, ISSATK 2024, 1–6. doi:10.1109/ISSATK62463.2024.10808494.